Summer Students Report 2023

August 11, 2023

Test of the first RPC-BIL prototype in view of the Mechanics Final Design Review

Supervisors: Alessandro Rocchi & Alessia Bruni
Summer Student: Jessica Dichakdjian

Abstract

In view of the HL-LHC luminosity increase, (7×10^{34} $cm^{-2}s^{-1}$ @ 14 TeV p-p, $\langle\mu\rangle$ =200) the Atlas Muon-Trigger needs significant upgrades. The RPC system will be upgraded adding 272 new generation RPC detectors in the Barrel Inner and replacing the old on detector trigger PADs with new DCTs.

The upcoming upgrade will bring significant enhancements to the system. It will increase trigger redundancy by expanding from 6 to 9 layers, resulting in heightened reliability. Acceptance will see a remarkable improvement, surging from 78% to 92%, reaching an impressive 96% with BI-BO coincidence. The spectrometer lever arm will be extended from 2.3 meters to 4.5 meters, enhancing measurement accuracy. Additionally, the upgrade will lead to improved tracking and trigger capabilities, while time resolution for TOF measurements will be notably refined.

I. The RPC detector

Resistive Plate Chambers (RPCs) are gaseous detectors designed in 1981, and since then, they have undergone significant advances in development, becoming a prevalent choice in high-energy and astroparticle physics experiments.

This detector uses two parallel plates with a gas-filled gap in between. When a particle passes through, it creates ions and electrons in the gas. An electric field accelerates electrons towards one plate, causing them to create more electrons through secondary ionization of the gas, resulting in an amplified signal. This signal indicates the particle's passage and is measured by electronics, making RPC detectors useful for tracking charged particles in various applications.

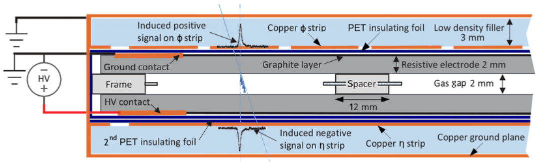

Figure 1 - RPC detector layout

As shown in Figure 1, the RPC detectors are composed of two high-pressure laminate (HPL) phenolic electrodes spaced through 1-2mm thick insulating pillars.

The volume between the electrodes is filled with Freon based gas mixture and the external surfaces of the electrode are coated by thin layers of graphite paint. The graphite has a surface resistivity of ~ 100 kΩ/sq, thus allowing uniform distribution of the high voltage along the plates without creating any Faraday cage that would prevent signal induction outside the plates. The high voltage on the graphite coatings produces an intense uniform electric field within the gas volume.

Figure 2 – RPC gas volume

These electrodes are made from a blend of phenolic resins, commonly known as Bakelite, with a volume resistivity (ρV) ranging from 10^9 to 10^{12} Ωcm. The plates are separated by insulating spacers, and the thickness of the plates and the gap between them, known as the gas-gap, can be adjusted based on experiment demands. In the ATLAS experiment, Legacy RPCs are equipped with plates that are 1.8 mm thick and spaced 2 mm apart, along with cylindrical spacers of 12 mm diameter placed approximately every 10 cm in both directions.

The inner surfaces of the Bakelite plates must exhibit exceptional smoothness achieved by applying a thin layer of linseed oil. Discharge electrons resulting from secondary ionization travel within the gas gap, and the signal induced through a capacitive coupling on external pick-up copper strips is collected by front-end electronics. In the ATLAS experiment, Legacy RPCs are designed with pick-up strips about 30 mm wide, organized into two orthogonal directions (η and φ panels). The eta & phi coordinates describe the hit position within the ATLAS Muon spectrometer.

II. RPC-BI upgrade

i. Upgrade description and goals

The goal of the BI system upgrade is to enhance trigger acceptance and efficiency by adding a layer of new-generation RPC chambers in the Barrel Inner region. The new BI RPC chambers will feature three independent RPC detectors and necessitate coincidences in at least two out of three planes for optimal efficiency and reduced random coincidences. The redesigned RPC technology includes thinner 1 mm gas gaps and 1.4 mm electrodes, as well as a low-noise high-sensitivity amplifier with a 2 fC threshold, resulting in improved rate capability and aging behavior (charge per count reduced by one order of magnitude). The upgraded RPCs will be integrated into the ATLAS detector, occupying tight spaces (about 6 cm thick detectors), and providing high trigger acceptance (about 96%). Additionally, they operate at a lower voltage (5600 V) and have increased rate capability (10 kHz/cm^2) while remaining cost-effective.

ii. New front-end electronics

To achieve these improvements, a new front-end electronics system was developed to amplify and discriminate avalanche signals. This new FE consists of the embedded preamplifier and discriminator with a minimum threshold of 0.3 mV (minimum detectable signals of 1 to 2 fC), and a Time-to-Digital Converter (TDC) with 100 ps resolution. Prototype tests have successfully demonstrated the efficiency and time resolution of the upgraded RPCs. The transition to the new integrated front-end ASIC is expected to significantly enhance the RPC system's performance, reduce costs, and increase radiation hardness.

iii. Detector design

The new RPC-BI gas volume comprised several key modifications. The gas-gap thickness was reduced from 2 mm to 1 mm improving the time resolution to 0.35 ns and reducing the HV working point from 9600 V to 5600 V. The bakelite electrode thickness is now 1.4 mm, and as described in Figure 3, a new HV connection on the gas volume side and new gas distributors on short sides with 2 inlet and 2 outlet ports have been designed.

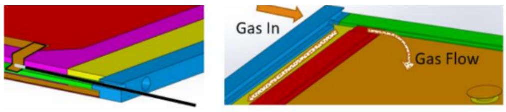

Figure 3 - Gas volume design

The readout panel design was redesigned, featuring an Eta-Eta readout due to the Atlas Muon Spectrometer layout. For this reason, the ϕ coordinate will be reconstructed through time differences between the two eta panels with 1 cm precision.

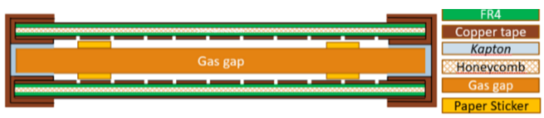

Figure 4 - The structure of the readout panel design

The read-out panel structure, as shown in Figure 4, consists of a sandwich of aramid paper honeycomb between copper glade halogen-free FR4 photoengraved plates with a total thickness of 3.8 mm.

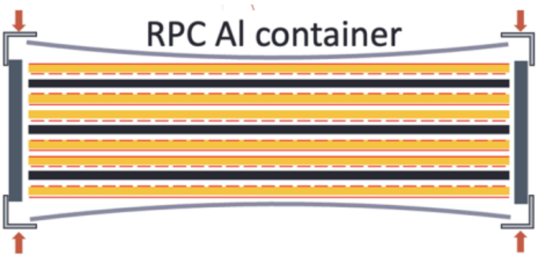

Figure 5 – RPC Al container

The BI chamber structure as described in Figure 5 evolved from two independent detectors with eta-phi readout to three singlet detectors with eta-eta readout, which improved trigger redundancy.

III. The RPC-BIL detector description

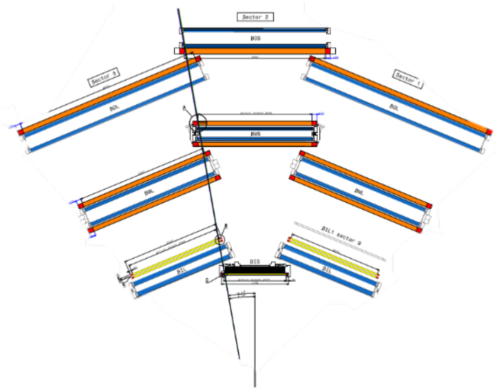

Figure 6

The RPC-BIL chambers are essential components housed within the large sectors of the spectrometer, serving a crucial role in the detection process. The original BIL frame design assumed a triplet thickness between 36 and 39 mm. [1]

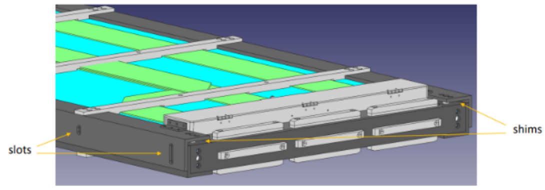

Figure 7 – BIL Triplet chamber

Two mechanical prototypes, denoted as v0.1 and v0.2, have been developed in different locations, namely Rome and Protvino. It's worth noting that while the dimensions of these prototypes differ slightly from the final specifications (width 670 instead of 680), their tolerances remain consistent. These prototypes have been integrated alongside singlet prototypes and services to enhance overall functionality.

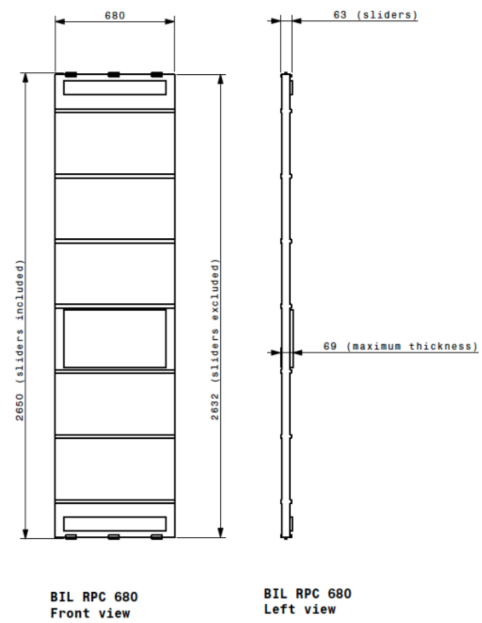

Figure 8 - BIL RPC dimensions

The mechanics are set up in a way that makes sure the gas volume can function properly, even if some parts aren't securely glued together. This is done by using slightly pre-bent aluminum plates that push on the surfaces of the gas volume. These plates help keep everything in place and working, even if some parts aren't tightly sealed. This smart design makes sure the RPC-BIL chambers can keep working even if some pieces aren't perfectly stuck together.

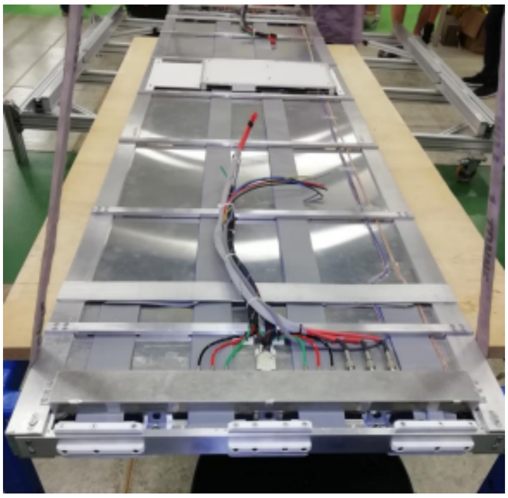

Figure 9- prototype from Rome

The RPC chamber design features 32 strips along the long side of each read-out panel, totaling 64 read-out channels. This configuration, however, poses a challenge in directly measuring ϕ coordinate. To address this, a method known as the Time Of Flight (TOF) method is employed. The TOF method involves reconstructing ϕ hit position based on hit times measured on each panel. This technique effectively mitigates the common jitter caused by RPC time resolution, resulting in improved spatial resolution. With a resolution of 100 ps, an expected spatial resolution of approximately 1 cm can be achieved. Refer to Figure 10 for a visual representation of this process.

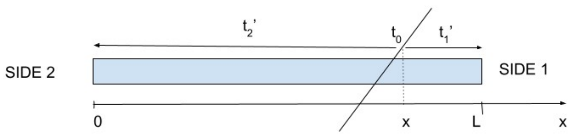

Figure 10 – Phi coordinate position reconstruction

Measuring the spatial resolution is a crucial preliminary step in the reconstruction of the ϕ coordinate. This measurement holds significance in the context of the Mechanics Final Design Review and the subsequent uniformity test. To ensure accurate results, the uniformity test involves the use of two scintillators, each 2 cm wide and spaced 6 cm apart.

This configuration helps reduce the projection on the detector, enhancing the reliability of the test. The TDC Caen V1190A is utilized for data acquisition during these tests. Additionally, ongoing tests involve applying a 2 mbar overpressure to half-glued gas volumes, further validating the uniformity check.

In this context, "half-glued" implies that the gas volumes are not fully sealed but rather partially secured with adhesive, which might lead to some variations in their behavior or properties.

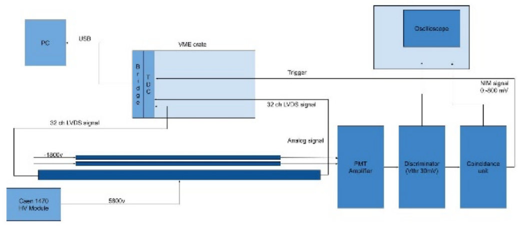

Figure 11 – The process of the trigger detector

The FE channels are integral to the system, connecting to the first 64 channels of the Caen V1190 TDC. This arrangement designates channels 0 to 31 for side 1 and channels 32 to 63 for side 2. An illustrative example can help clarify this connection: if a particle were to impact the 11th channel on side 1, the 42nd channel on side 2 would also register a signal (31 + 11). The TDC records the following information:

TDC_Channel: 10, 42
TDC-TimeStamp: t_1, t_2
Trigger_time: t_t

x=0	$t_2 = 0 + t_t$ $t_1 = t_1' + t_t$	$\Delta t = - t_1'$
x=L	$t_2 = t_2' + t_t$ $t_1 = 0 + t_t$	$\Delta t = t_2'$

These equations are applicable when the particle beam crosses the detector at the extremities of each side. These calculations allow us to analyze the distribution of hits across various positions.

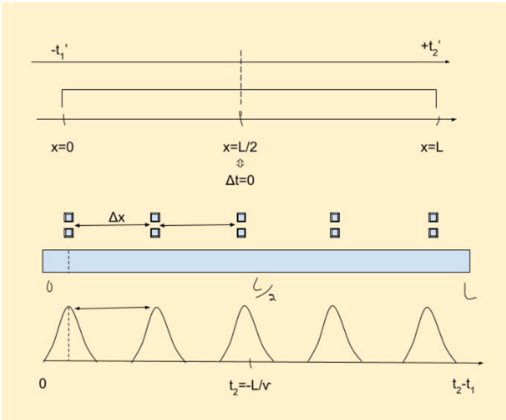

Figure 12 – Number of hits on each position

From the derived graphs, we can formulate the following equations.

$$\Delta x = \frac{L}{2} - \frac{v}{2}(t_2 - t_1) = \begin{cases} 1)\ \frac{L}{2} - v.\frac{t_2}{2} = L \\ 2)\ \frac{L}{2} \\ 3)\ \frac{L}{2} - v.\frac{t_1}{2} = 0 \end{cases}$$

The first equation corresponds to the scenario where t_1 is zero and t_2 is $-L/v$, the second equation applies when t_2 and t_1 are equal, while the third equation is relevant when t_2 is zero and t_1 is L/v

Moving to the determination of eta and phi coordinates, we find that for the eta direction (parallel to the short side), the coordinates can be directly measured from the channels that register hits. However, for the phi direction, readout strips are not available. Instead, the time of flight measurement methodology is employed to construct the points corresponding to the path taken by particles.

IV. Test of the RPC-BIL prototype for the MFDR

i. Aim of the test

Testing occurred in bb5.

The aim of the test is to ensure reliable detector functionality within scenarios of potential gas volume damage, emphasizing the role of mechanical frames. Essential to these frames are spacers, connecting the electrodes and maintaining a consistent 1mm gas gap. These mechanical components rely on external, pre-bent aluminum plates, exerting force to press the electrodes against the spacers (also referred to as pillars). This mechanism guarantees that even in cases of unglued spacers, the gas gap's thickness remains unaltered. The test was conducted using the BIL RPC type, and to address this issue, a deliberate decision was taken to create a "broken" RPC detector with one electrode unglued from the pillars.

The perimetral corner frames are glued to both electrodes ensuring gas tightness. This configuration allows the electrodes to accommodate mechanical stresses imposed on the detector, encompassing torsion or heightened pressure within the gas volume.

The measurement of the detection uniformity also in the case of pressurization of the gas volume allows us to evaluate the correct functioning of the containment structure. Any non-uniformity can be attributed to the potential bending of the electrode, leading to deformation and consequently disrupting gas gap uniformity. In this scenario, the distance between the electrode and the opposing counterpart could vary, with the minimum separation being the thickness of the spacer, and the maximum reaching the greatest extent of electrode bending.

As stipulated by the Technical Design Report [1], detecting non-uniformity with pressure exceeding 2 mbar within the gas volume does not pose an issue, considering the detector's design parameters do not accommodate pressures surpassing this threshold. However, if non-uniformity is identified under pressures lower than 2 mbar, it indicates a potential flaw in the mechanical frame's agreement with the experiment's specifications.

ii. Test description

We inserted this broken detector within the mechanical frames and studied the response along the hole detector surface. For testing purposes, scintillators were employed as trigger detectors, initially with two on the upper section and one on the lower section, as described in Figure 13. During the test, technical issues emerged with the bottom photomultiplier tube hitting the detector support, so we decided to remove this scintillator from the trigger, as shown in Figure 16. This implied the rate of the event increased because the acceptance of the trigger was higher, but we couldn't measure the detector efficiency. For this reason, we just measured the hits rate along the hole detector surface, in the following configurations:

- 0 mbar within the gas volume
- +2 mbar within the gas volume

To verify the hits rate uniformity, we compared the experimental results with simulated hits distribution.

Figure 13 - Slight bending of the detector

Figure 14 – issue with the photomultiplier tube of the bottom scintillator

In Figure 15, you can see the difference in the angles of the particles crossing when the detector has 3 scintillators and 2 scintillators.

When there are 3 scintillators, the angle of the particles crossing is smaller, we are covering the highlighted area, the acceptance is full, and we didn't select particles that go outside the areas of the RPC (the red lines in the figure). When there are only two scintillators because the third one has to be removed since its photomultiplier doesn't fit, particles could have a higher angle, which means there are more particles selected from the trigger. This increases the rate of the detector covering a bigger area of the RPC, but particles sometimes go outside of the RPC, which means not all the events triggered hit the RPC (the black lines in Figure 15).

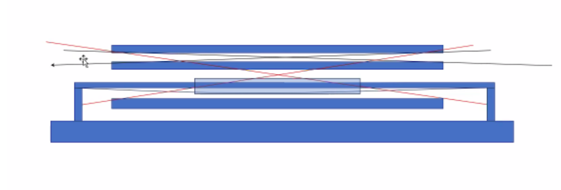

Figure 15 – The cross angles of the particles

The fraction of these kinds of particles in an event is low just because these particles arrive from cosmic rays to the ground following a low distribution angle, which goes in accordance with the cosine distribution law. This law states that there is a high probability for particles to come from a vertical angle and a very low probability of having particles parallel to the ground. Assuming a flat Earth, the particle flux as a function of the Zenith angle θ follows with good approximation the distribution $\cos^2\theta$.

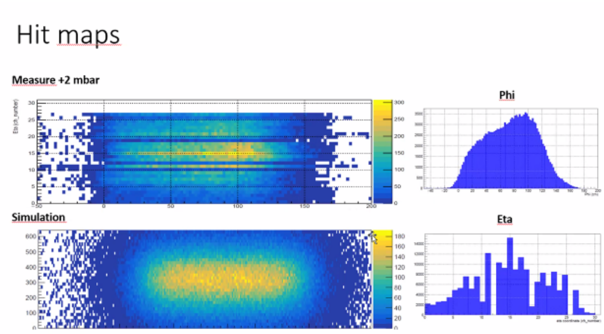

Figure 16

iii. Strip line signal drift velocity measurement

Experimental setup

It is composed of a trigger system, Consisting of 2 scintillators. The scintillators are 20 cm wide, 115 cm long and 5 cm thick; they are positioned over the chamber parallel to the long side of the RPC. The signal of the scintillator is discriminated with a Lecroy 623 module with a threshold of 50 mv. Then the signals are used to produce a coincidence that is the trigger for our Data acquisition. The data acquisition system consists of a Caen V1190 TDC connected to the PC through the Caen V1718 VME bridge.

Flux Diagram of TDC

iv. Uniformity measurements

The setup closely resembles the stripline experiment used for measuring signal drift velocity, differing primarily in the scintillator sizes employed.

In this configuration, the utilization of larger scintillators introduces a departure from double coincidence's full acceptance assurance and efficiency measurement limitation. However, it facilitates coverage over a more substantial portion of the detector surface and a boost in statistical data, enabling a more time-efficient execution of the test.

v. Results from the measurements

The plot in Figure 18 shows the Gaussian fits of the reconstructed phi coordinate position with the time of flight, in the case in which the trigger was constituted by the small scintillators.

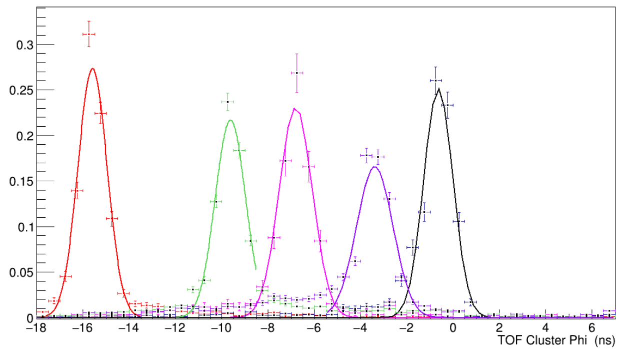

Figure 17- The Gaussian fits of the reconstructed phi coordinate position with the time of flight

Comparing the scintillator positions to the time-of-flight distribution, we measured the average value of drift speed of the signal propagation along the strip lines as 20.7 cm/ns. The drift speed can be used as a scale factor to convert the time information to reconstruct the hit position.

The width of the distributions allows us to evaluate spatial resolution. With a sub-millimeter resolution, the distributions should describe the hit probability distributions fixed by the scintillator's width and configuration. In that case, the distributions are worsened by a systematic time of flight shift between the various channels, probably linked to a problem in the prototype version of the FE card, but by evaluating the distribution of the hits on individual channels it is possible to resolve the width of small scintillators (refer to the plot of figure 19).

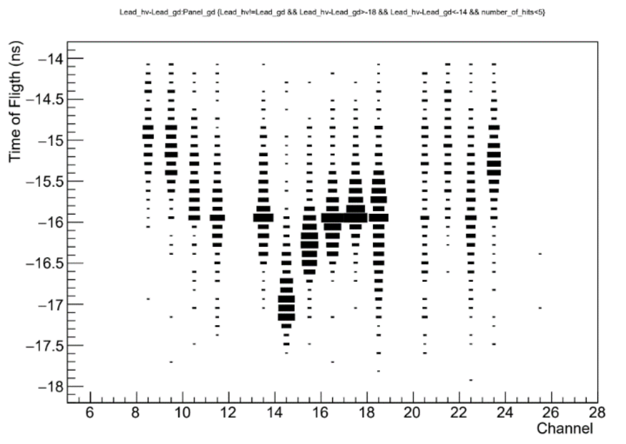

Figure 18- finger map

Figure 20 instead shows the hit map on the chamber for three different cases:

1. No overpressure
2. +2mbar of overpressure
3. No overpressure with the scintillators turned by 180°

The last case was studied to evaluate if the non-uniformities were due to the trigger.

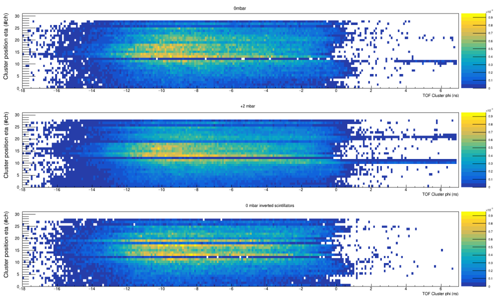

Figure 19 - Hit map on the chamber for 3 cases

Non-uniformities are observed in the hit map that is not in agreement with the simulation. However, these non-uniformities are not related to the trigger or the applied overpressure and are still under study.

V. Conclusions

In conclusion, our experimental investigation has yielded valuable insights into the spatial resolution and distribution of signal propagation in the scintillator-based system. The analysis has established an upper limit on the spatial resolution, approximately 2 cm, demonstrating the system's capability to localize hits with a high degree of precision.

Furthermore, the results indicate that the distribution of spatial resolution remains consistent regardless of variations in overpressure. Despite the non-uniformities observed in the hit map, it is evident that these discrepancies are not attributed to the trigger mechanism or the introduction of overpressure.

The ongoing efforts are focused on comprehending the origins of these non-uniformities and refining our system to align with simulation expectations. Through this endeavor, the aim is to enhance the accuracy and reliability of our scintillator-based setup for future applications.

Citation

1. BIL mechanics constraints on singlets by M. Corradi, A. Pelosi
2. ATLAS Collaboration. "Technical Design Report for the Phase-II Upgrade of the ATLAS Muon Spectrometer" by the ATLAS Collaboration